Radiation response of *n*-type base InP solar cells

Robert J. Walters[a)]
U.S. Naval Research Laboratory, Code 6825, 4555 Overlook Avenue SW, Washington, DC 20375

S. R. Messenger
SFA, Incorporated, Largo, Maryland 20774

G. P. Summers[b)]
U.S. Naval Research Laboratory, Code 6825, 4555 Overlook Avenue SW, Washington, DC 20375

M. J. Romero and M. M. Al-Jassim
National Renewable Energy Laboratory, 1617 Cole Boulevard, Golden, Colorado 80401-3393

D. Araújo and R. Garcia
Departamento de Ciencia de los Materiales e IM y QI Universidad de Cádiz, Apartado. 40, E-11510, Puerto Real (Cádiz), Spain

(Received 23 January 2001; accepted for publication 11 July 2001)

The effects of particle irradiation on the electrical properties of high efficiency p/n InP solar cells have been studied using a variety of techniques including current–voltage and spectral quantum efficiency measurements (QE), electron beam induced currents (EBIC), and deep level transient spectroscopy. A detailed analysis of the radiation response of the solar cell photovoltaic response is presented, and the primary damage mechanisms are identified. Data measured after irradiation by protons of various energies are correlated in terms of displacement damage dose to produce a characteristic degradation curve for the p/n InP technology. This characteristic curve is compared to that of the n/p InP technology to provide an assessment of the relative radiation hardness of the p/n devices. Radiation-induced decreases in the minority carrier diffusion length in both the *p*-type emitter and *n*-type base at low damage levels have been extracted from the QE and EBIC measurements, and damage coefficients have been determined. At high damage levels, EBIC profiles suggest that the primary device degradation mechanism is an increase in bulk resistivity due to electron trapping in the base. However, capacitance–voltage measurements did not indicate any change in the junction capacitance. A model to account for these effects based on radiation-induced defect kinetics is presented. © *2001 American Institute of Physics.* [DOI: 10.1063/1.1398592]

I. INTRODUCTION

The primary degradation mechanism in space solar cells is displacement damage caused by protons and electrons trapped in the radiation belts of the Earth or ejected in solar events. Thus, an important property for a space solar cell is the electrical conversion efficiency at the end of the mission life, commonly referred to as the end-of-life efficiency. An attractive space solar cell technology, therefore, is one that displays both high efficiency and superior radiation resistance. InP solar cells have been shown to be such a technology,[1,2] but due to the cost and fragility of InP wafers, InP solar cells have not yet found wide use. To circumvent these limitations, attempts have been made to grow InP solar cells on Si wafers, although the efficiencies obtained to date in such cells have been somewhat low.[3]

Until recently, most efforts to develop InP cells has been focused on cells with a *n*-type emitter and a *p*-type base, i.e., the n/p polarity, due to difficulties in passivating and attaining high dopant levels in *p*-type InP emitters. It would be advantageous, however, in producing InP/Si cells if the active InP region could be fabricated in the p/n polarity, since this would eliminate the need for a tunnel junction at the InP/Si interface to overcome the counter diode formed by Si autodoping in InP. The p/n polarity would also reduce device sensitivity to the effects of high, emitter surface-recombination velocity.[4] Recently, Hoffman *et al.*[4] have demonstrated the capability of controlling the growth of *p*-type InP emitters and thereby of producing for the first time p/n cells with efficiencies comparable to those with the n/p polarity.

The present article reports a detailed study of the radiation response of these cells and p/n InP solar cells produced in two other laboratories, which combines electron beam induced current (EBIC) data with illuminated current versus voltage ($I-V$), spectral quantum efficiency (QE), and deep level transient spectroscopy (DLTS) measurements.

II. EXPERIMENTAL DETAILS

Solar cells fabricated in three different laboratories were studied: Essential Research Inc. (ERI), Spire Corporation, and the Research Triangle Institute (RTI). The Spire and RTI cells were grown under contract with the U.S. Naval Research Laboratory (NRL). The ERI cells were supplied under a Cooperative Research and Development Agreement be-

a)Electronic mail: rwalters@ccf.nrl.navy.mil
b)Also at: Department of Physics, University of Maryland, Baltimore County, Baltimore, MD 21225

TABLE I. Configuration of the three p/n InP/InP solar cell structures studied here. Cells in configuration B and C had step-graded emitters as indicated.

Configuration	Manufacturer	Emitter		Base	
		Thickness (μm)	Dopant level (cm^{-3})	Thickness (μm)	Dopant level (cm^{-3})
A	Spire	0.15	2×10^{18}	3	3×10^{16}
B	RTI	0.15	2×10^{18}	3	5×10^{16}
		0.05	5×10^{17}		
		0.05	3×10^{17}		
		0.05	5×10^{16}		
C	ERI	0.04	1×10^{18}	2	1.5×10^{17}
		0.11	7×10^{17}		

tween NRL and ERI. The internal structure of the devices is summarized in Table I. All of the cells were grown by metalorganic chemical vapor deposition on *n*-type, Si-doped, InP wafers and include a heavily doped back surface field layer. In all three cases, the base dopant species was Si, and the emitter dopant species was Zn. The most significant variation among the three cell configurations is the emitter structure. In configuration A, the emitter was 0.15 μm thick and uniformly doped to a level of about $2\times10^{18}\,cm^{-3}$. In configuration B, the emitter was thicker by a factor of 2, but the dopant profile was step graded from 2×10^{18} down to $5\times10^{16}\,cm^{-3}$. In configuration C, the emitter was 0.15 μm thick with a two-step dopant profile.

The photovoltaic response of the solar cells was measured using an Oriel 1000 W Xe Arc Lamp Solar Simulator with AM0 filtering. The simulator intensity was adjusted to 1 sun intensity using an InP reference cell calibrated on the NASA Glenn Lear Jet facility. The spectral response measurements were made using a standard lock-in amplifier system, and the DLTS measurements were made using a BioRad DL4600 system, which employs a Boonton 72B capacitance meter.

For EBIC measurements, the cells were mounted on a modified sample holder of a JEOL-JSM820 scanning electron microscope. The EBIC signal, from which the minority carrier diffusion length was determined using finite element analysis,[5] was measured with the electron beam incident normally upon the top surface of the cell [Fig. 1(a)]. In this configuration, the EBIC gain, i.e., the ratio of the EBIC signal to the incident electron-beam current, could be recorded with different electron-beam acceleration voltages between 1 and 30 keV to give information as a function of depth into the device. In other experiments, the electron-beam was scanned across a freshly cleaved {100} face perpendicular to the solar cell epilayers [Fig. 1(b)] so that EBIC profiles could be recorded.

The solar cells were exposed to various proton irradiations at either the Pelletron facility at the Naval Surface Warfare Center in Silver Spring, MD (now located at Carderrock, MD) or at NRL. The proton energies employed ranged from 1 to 5 MeV. Each solar cell was exposed to irradiation by protons at only one energy. In some experiments, the irradiations were performed incrementally with the devices being electrically characterized after each fluence increment. For analysis, the particle fluences were converted to displacement damage dose (Dd) using the appropriate nonionizing energy loss (NIEL), according to the formalism developed by Summers *et al.*[6]

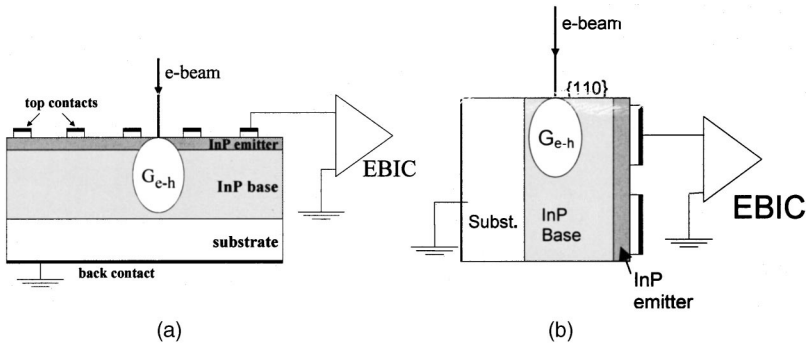

FIG. 1. Schematic diagram of the mounting configurations for the EBIC measurements is shown. The devices are mounted on an adapted holder of a JEOL-JSM820 scanning electron microscope. The configuration for measurements made with the electron-beam incident normally upon the cell surface is shown in (a). In this configuration, the EBIC gain was measured with increasing acceleration voltages to produce data as a function of depth into the cell. The mounting for cross sectional measurement is shown in (b) where the electron beam is scanned across a freshly cleaved {110} surface.

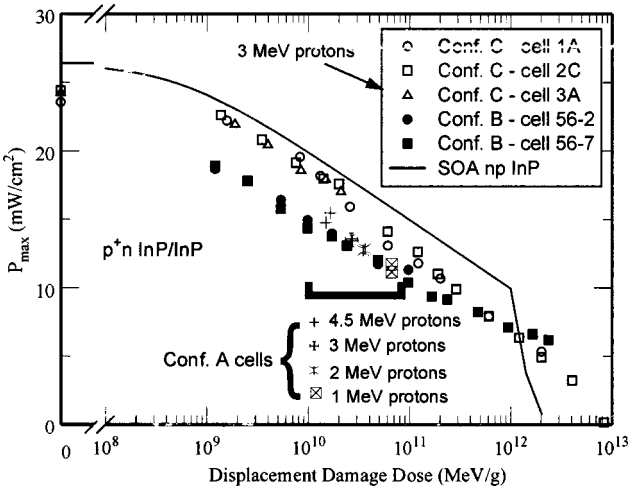

FIG. 2. Plot of the maximum electrical power output (P_{max}) of p/n solar cells after proton irradiation is shown. The data are plotted as a function of displacement damage dose (Dd) given by the product of the particle fluence with the NIEL (Ref. 6). The legend identifies the p/n cells according to the internal cell structure as described in Table I. Also shown are data from a state-of-the-art (SOA) n/p InP/InP solar cell (Ref. 3). The data from cells in configuration C closely track those of the SOA n/p device, indicating relatively good radiation resistance. The collapse of the n/p cell output at high Dd levels is caused by the effects of carrier removal, but these effects are not evident in the p/n cell data.

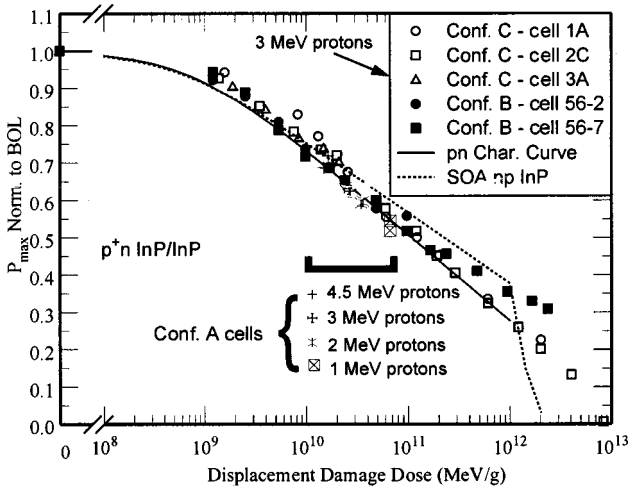

FIG. 3. The data of Fig. 2 normalized to the respective preirradiation values are shown. All of the p/n data collapse to a single curve as a function of Dd (represented by the solid curve) independent of the irradiating proton energy or specific cell configuration. Following the methodology of Summers *et al.* (Ref. 6), this curve can be considered characteristic for the p/n InP technology and can be used to predict the cell response to irradiation by protons of any energy or by a spectrum of energies as encountered in space. The fact that the p/n characteristic curve is essentially independent of the initial cell performance suggests that this radiation characteristic will be maintained even as the initial solar cell performance is further improved. Considering that the p/n characteristic is only slightly below that of the proven radiation hard SOA n/p device (Refs. 1 and 2), these results bode very well for future p/n InP devices for space applications.

III. EXPERIMENTAL RESULTS

A. IV measurements

A plot of the response of the maximum power output (P_{max}) of the p/n InP solar cells to proton irradiation is given in Fig. 2. Also shown for comparison are data from a state-of-the-art (SOA) n/p InP/InP solar cell.[2] The beginning-of-life (BOL) P_{max} values for the cells in configuration C were, on average, ~24 mW/cm^2. This is about 20% higher than the other devices (~20 mW/cm^2) and only about 8% less that than that of the SOA n/p devices (~26 mW/cm^2). Note that, as expected from the formalism of Summers *et al.*,[6] the data measured after irradiation by protons of various energies correlate directly in terms of Dd.

In Fig. 3, the radiation data have been normalized to the respective BOL values and then plotted as a function of Dd. When plotted in this fashion, all of the data collapse to essentially the same curve, which therefore, can be considered characteristic for the p/n technology. The solid curve in Fig. 3 represents a fit of the p/n data to the standard expression given in the Solar Radiation Handbook,[7] expressed as a function of Dd rather than fluence. For Dd levels less than about 1×10^{12} MeV/g, the p/n curve lies only slightly below the n/p curve. Considering the proven radiation hardness of the n/p InP devices[1–3] this indicates excellent radiation tolerance for the p/n cells as well. Furthermore, for higher Dd levels, the p/n devices show better performance than the n/p cells. In particular, the collapse of the n/p cells at a Dd of about 2×10^{12} MeV/g due to carrier removal effects[8,9] does not seem to be evident in the p/n cells.

The response of the p/n solar cell open circuit voltage (V_{oc}) to proton irradiation is shown in Fig. 4. Prior to irradiation, the cells in configurations A, B, and C displayed average V_{oc} values of 0.840 V, 0.820 V and 0.860 V, respectively. Considering cells in configuration C, this is only ~2% less than that of the best n/p cells. Overall, the radiation response of V_{oc} of the p/n cells appears to be superior to that of the n/p cell, especially in the higher Dd regime where the n/p cell voltage collapses at a much lower Dd level. Also, when plotted on a normalized scale, all of the p/n data collapse to a single curve, so that, as just discussed, this degradation curve is characteristic for the p/n InP technology.

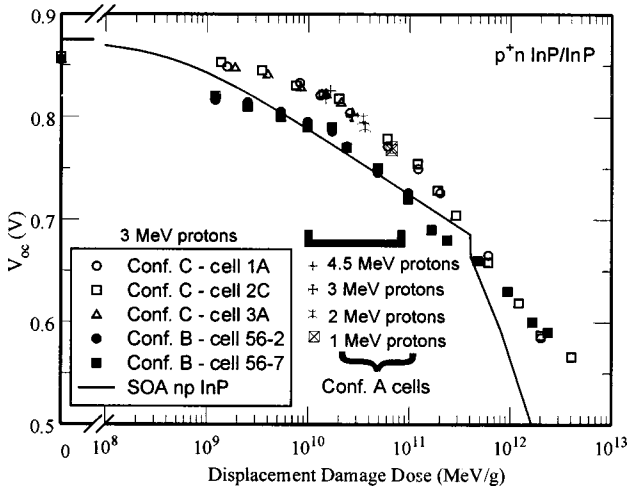

FIG. 4. The degradation of the V_{oc} of the p/n InP solar cells due to proton irradiation is shown. The solid curve represents data from a SOA n/p InP solar cell (Ref. 2). The radiation response of the p/n cells is superior to that of the n/p cells, especially at the very high Dd levels where carrier removal causes the collapse of the n/p cells.

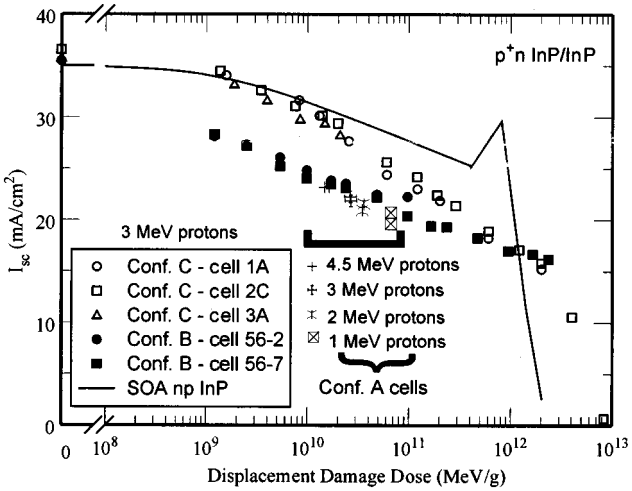

FIG. 5. The degradation of the short circuit current (I_{sc}) of the p/n InP solar cells due to proton irradiation is shown. The solid curve represents data from a SOA n/p InP solar cell (Ref. 2). The preirradiation performance of the configuration C cells is essentially equal to that of the n/p cell, but these cells appear to degrade more rapidly under irradiation.

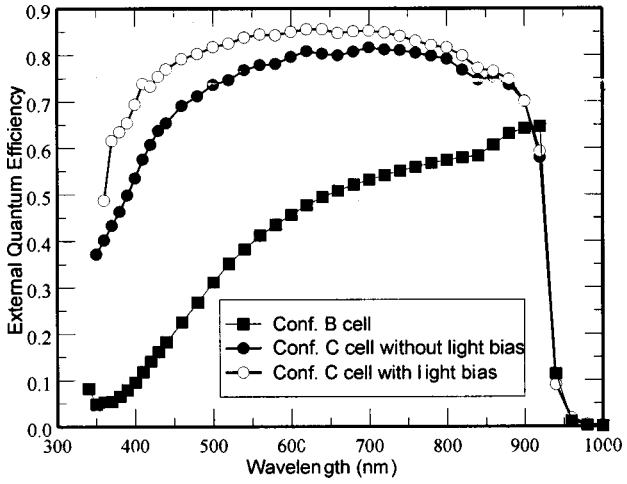

FIG. 6. Spectral response measurements made on the p/n solar cells prior to irradiation is shown. Light biasing was achieved by illuminating the cell with a 541 nm He(Ne) laser during the measurements. The response of the configuration C cell is especially good at shorter wavelengths indicating efficient current collection from the emitter. Applying the light bias caused the cell response to increase further, with the increase being more pronounced at shorter wavelengths. This is thought to occur as a result of photogenerated charges passivating interstitial Zn defects in the emitter region, as investigated further in Fig. 7.

The effect of proton irradiation on the short circuit current (I_{sc}) of the p/n cells is shown in Fig. 5. Prior to irradiation, cells in configurations A and B displayed I_{sc} values around 30 mA/cm^2. The preirradiation I_{sc} of the cells in configuration C were ~36 mA/cm^2, which is essentially equal to that of the best n/p cells. However, the I_{sc} of the configuration C cells degrades more rapidly under irradiation than that of the other cells. The abrupt increase and subsequent decrease to zero observed in the n/p cell data is due to the effects of carrier removal,[8,9] which are not apparent in the p/n cell data.

B. QE measurements

Typical QE measurements made before irradiation on solar cells in configurations B and C are shown in Fig. 6. For the configuration C cell, two data sets are shown—one measured with and the other without a light bias. The light bias was achieved by illuminating the cell with a 541 nm He(Ne) laser during the measurement. The configuration C cell displays better response, especially at shorter wavelengths, and the light bias resulted in a further increase in the short wavelength response. These data have been fit to the equations of Hovel[10] from which the response of the emitter, base, and depletion regions have been estimated. Examples of the fitting results are shown in Fig. 7. The results indicated that the increased short wavelength response could be attributed almost exclusively to increase in the emitter response, and in particular, to an increased emitter diffusion length. The increase in emitter response with the application of a white-light bias has been attributed to the passivation of Zn interstitial defects.[4]

QE measurements were made on the p/n solar cells after irradiation with incremental fluences of 3 MeV protons. A set of QE curves measured in a configuration C cell with light bias is shown in Fig. 8. These data were also fit to the Hovel equations[10] where the effect of the irradiation was modeled as a decrease in minority carrier diffusion length in the base and emitter. Reasonable fits of the measured data were obtained for Dd levels up to 2×10^{12} MeV/g. The diffusion length values obtained from the fits are shown in Fig. 9. This analysis was also performed using data measured in a configuration B cell, but because these measurements were made without a light bias, only the base diffusion length data are included.

The decrease in diffusion length with increasing Dd was found to be described reasonably well by the standard expression:[7]

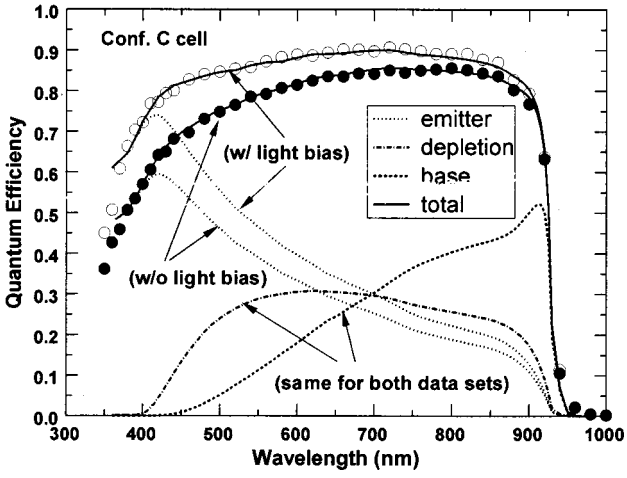

FIG. 7. Analysis of the spectral response data from a configuration C cell prior to irradiation measured both with and without a light bias is shown. The data have been fit to the equations of Hovel (Ref. 10) from which an estimate of the response of the emitter, depletion region, and base are obtained. For both data sets, the fits produced essentially the same depletion region and base response, while the emitter response was found to be significantly higher for the data taken with light bias.

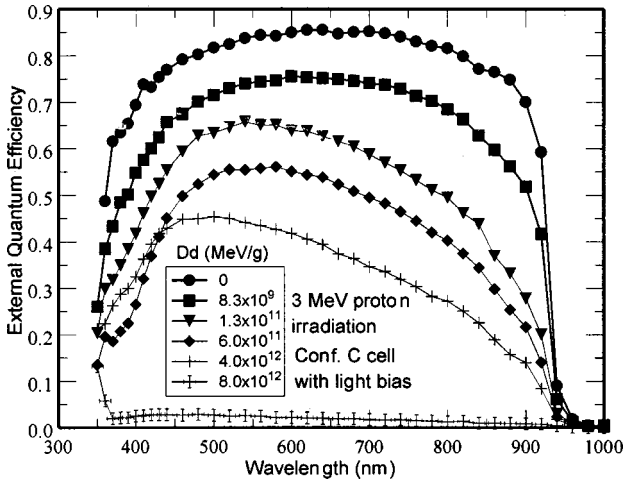

FIG. 8. Spectral response data measured with a light bias in a configuration C cell after irradiation with incremental fluences of 3 MeV protons is shown. For Dd levels up to 2×10^{12} MeV/g, the data were well described by the Hovel equations (Ref. 10) where the radiation-induced degradation was modeled through a decrease in the diffusion length in the emitter and base. At the higher Dd levels, however, the degradation of the cell response could not be accurately modeled by diffusion length degradation alone.

$$\left(\frac{1}{L(\mathrm{Dd})}\right)^2=\left(\frac{1}{L_0}\right)^2+K_L\mathrm{Dd}, \tag{1}$$

where L_0 is the preirradiation value and K_L is the diffusion length damage coefficient. A fit of the data to this expression (represented by the lines in Fig. 9) produced an estimate of K_L for the emitter and the base.

The degradation in the QE response after irradiation up to Dd levels above 2×10^{12} MeV/g could not be modeled by degradation in the diffusion length alone. Using diffusion length values obtained from an extrapolation of Eq. (1) to higher Dd values significantly overestimated the cell response. The data seem to suggest a change in the internal cell structure. However, in agreement with the $I-V$ parameter analysis, this structure change does not appear to be a result of carrier removal, as the sharp increase in depletion region response that would occur if the base became depleted was not observed.

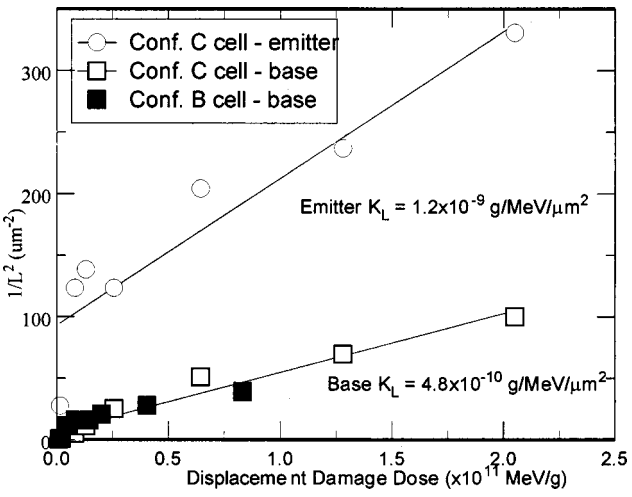

FIG. 9. Degradation of the emitter and base diffusion length as determined from fits of the Hovel equations (Ref. 10) to spectral response data measured with a light bias (Fig. 8) is shown. The lines represent a linear least squares fit of the data, from which a damage coefficient has been determined according to Eq. (4). Base diffusion length data from a configuration B cell is also shown, which was determined from spectral response data measured without a light bias.

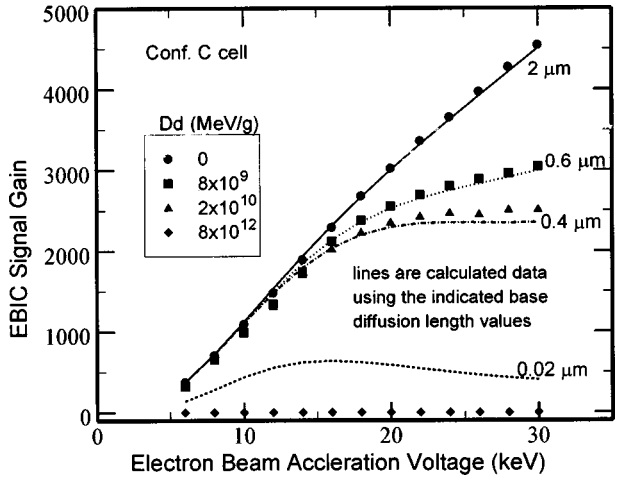

FIG. 10. EBIC data measured in configuration C cells after irradiation by 3 MeV protons are shown. These data were measured in the normal incidence configuration [Fig. 1(a)]. The symbols represent the measured data, and the lines show calculations made using the methodology developed at UCA.[5] In the calculations, the base diffusion length data predicted by Eq. (1) for each Dd level were used. The calculated data agree well with the measured data, except in the heavily irradiated case, where the calculations over estimate the cell response.

C. EBIC measurements

EBIC measurements were made on configuration C cells before and after irradiation with 3 MeV protons. EBIC data measured in the normal incidence configuration [Fig. 1(a)] as a function of electron beam acceleration voltage are shown in Fig. 10. The symbols in Fig. 10 represent the measured data, and the solid curves represent calculations made with various values of L_p. The calculations were made using the modeling routine developed at University of Cadiz (UCA).[5] For all but the highest Dd level, the calculations agree reasonable well with the measured data, and the estimates of L_p are in reasonable agreement with those obtained from analysis of the QE data. However, as found in the analysis of the QE data, modeling the EBIC response of the most heavily irradiated cell proved difficult. Using the damage coefficient determined in Fig. 9, the base diffusion length for Dd$=8\times10^{12}$ MeV/g is estimated to be about 0.02 μm, but using this value in the EBIC simulations significantly overestimates the cell response.

Cross sectional EBIC measurements [Fig. 1(b)] were made on freshly cleaved (100) surfaces of configuration C solar cells. As the electron beam was scanned across the cleaved edge, the EBIC signal was averaged laterally across the device and recorded as a function of position. Cross sectional EBIC micrographs thus measured in devices after proton irradiation up to two Dd levels (2×10^{10} and 8×10^{12} MeV/g) are shown in Fig. 11. The peak of the EBIC signal corresponds to the position of the p/n junction. At the lower Dd level, the EBIC signal was reduced from the preir-

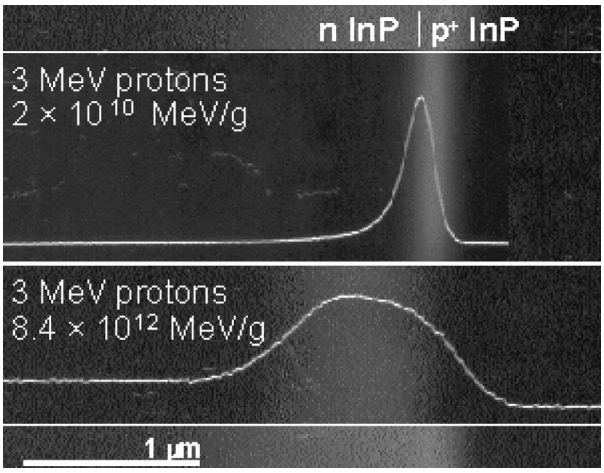

FIG. 11. EBIC images recorded in cross sectional view of configuration C solar cells [Fig. 1(b)] after 3 MeV proton irradiation is shown. Shown are average EBIC linescans superimposed upon the measured micrographs. The peak in the EBIC linescan indicates the location of the p/n junction. At a Dd level of 2×10^{10} MeV/g, the EBIC intensity was reduced from the pre-irradiation level (not shown), but the shape and location of the linescan peak was unchanged. At the higher Dd level, a significant broadening of the peak is observed, with the signal peak now located nearly 1 μm into the p-type base region.

radiation level (not shown), but the shape and position of the peak were unchanged. At the higher Dd level, on the other hand, the peak was much broader and appeared to extend almost 1 μm into the base.

Attempts to model the cross-sectional EBIC scans of Fig. 11 were made using the methodology developed at UCA[5] (Fig. 12). At the lower Dd level, a good fit was obtained assuming the diffusion length determined from Eq. (4)

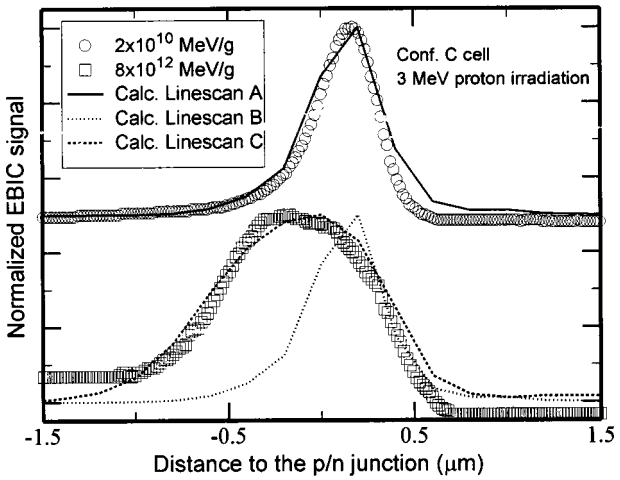

FIG. 12. Analysis of the cross sectional EBIC linescans of Fig. 11 is shown. Shown as the open symbols are the EBIC linescan data measured in a cell irradiated up to 2×10^{10} MeV/g and in another cell irradiated up to 8×10^{12} MeV/g. The lines are calculations made using the UCA methodology (Ref. 5). At the lower irradiation level, the base diffusion length obtained from Eq. (1) was used in the calculations, and a good match to the measured data was obtained. At the higher irradiation level, linescan B represents calculations made using the base diffusion length given by Eq. (4), and a poor fit to the measured data is observed. A much better fit is obtained with calculated linescan C, where in addition to the diffusion length reduction, a reduction in the base majority charge carrier concentration and mobility was included.

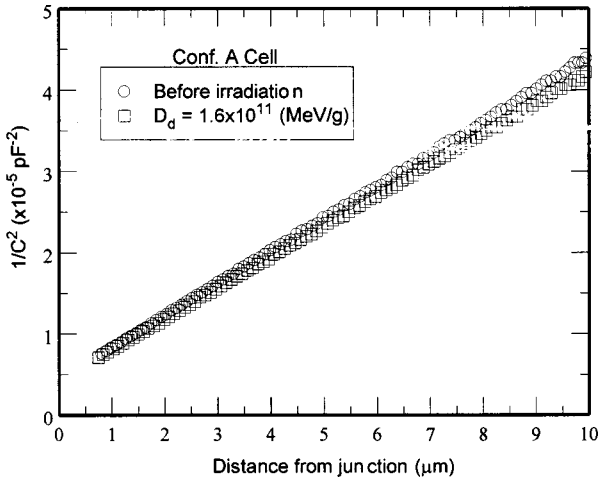

FIG. 13. Capacitance vs voltage measurements made in a p/n diode in configuration A before and after proton irradiation, plotted as the inverse square of the capacitance are shown. Within the one sided, abrupt junction approximation, the slope of these lines is expected to be inversely proportional to the majority charge carrier concentration in the base. After irradiation, a very small decrease in slope is observed.

(linescan A in Fig. 12). At the higher Dd level, calculations made using the diffusion length of 0.02 μm that is predicted by Eq. (1) yield a poor fit to the experimental data (linescan B in Fig. 12). To obtain a reasonable fit to the heavily irradiated data, it was necessary to also assume a reduction of the majority charge carrier density to $3\times10^{16}\,\mathrm{cm}^{-3}$ and an order of magnitude reduction in the base mobility (linescan C).

D. Capacitance versus voltage and DLTS measurements

Capacitance versus voltage ($C-V$) measurements were made on a p/n diode in configuration A before and after proton irradiation. In Fig. 13, the values of $1/C^2$ are plotted as a function of applied reverse bias. According to the abrupt-junction, parallel plate capacitor approximation,[11] the slope of these lines are expected to be inversely proportional to the base carrier concentration. The data show a small decrease in the slope after irradiation.

The radiation-induced DLTS spectra within the base region of the p/n InP solar cells after proton irradiation are shown in Fig. 14. In Fig. 14, a positive signal indicates majority charge carrier (electron) capture while a negative signal indicates capture of a minority charge carrier (hole). A total of four electron traps and one hole trap were detected, and the activation energy determined for each peak is shown. The peak position and activation energies of two of the electron trapping centers observed in the present samples, EB and ED, are quite similar to those of electron tapping centers observed as minority carrier traps in irradiated p-type InP[12,13] and are labeled accordingly. The hole trap observed here seems to correspond to the large H4 peak observed as a majority carrier peak in irradiated p-type InP.[1,12,13] Note that the H4 peak observed here is scaled by a factor of 25 to make it visible when plotted with the electron traps, indicating a relatively small defect concentration. This is consistent

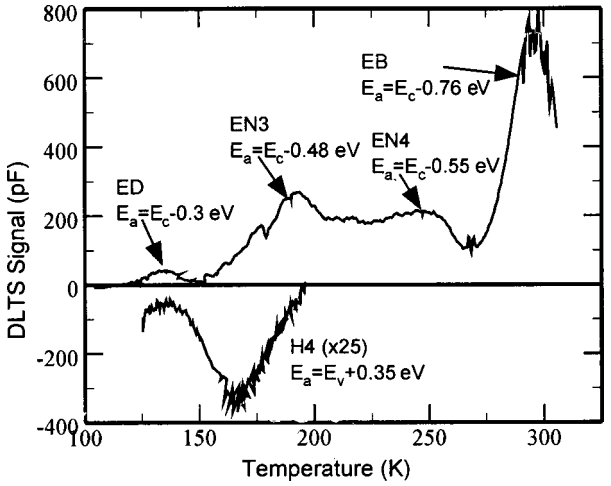

FIG. 14. Typical DLTS spectra measured in the *n*-type base of the p/n InP cells after proton irradiation are shown. A positive signal indicates majority charge carrier (electron) capture, and a negative signal indicates minority charge carrier (hole) capture are presented. The activation energy determined for each of the observed peaks is indicated. When possible, the peaks have been identified with peaks measured in irradiated *p*-type InP and labeled accordingly. The peak labeled H4 has been scaled by a factor of 25 to make it more visible.

with the *p*-type InP results since the H4 peak has been shown to be substantially reduced, but not completely removed by minority carrier injection and since the majority carrier trap DLTS scans in these p/n devices induces minority carrier injection at this defect level.

The electron trap peaks labeled EN3 and EN4 (E—for electron and N—for *n*-type material) could not be directly correlated with any data from *p*-type InP. It is possible that these peaks are present but not observable in the minority carrier trap spectrum of irradiated *p*-type InP. Given the location of these two peaks in the spectrum, they would be expected to lie almost directly below the peaks labeled H4 and H5 in the *p*-type majority carrier spectrum. Thus the positive signal from the H4 and H5 peaks would obscure detection of the negative signal from the EN3 and EN4 peaks. Furthermore, the EN3 and EN4 peaks were found to be removed by thermal annealing at ~360 K and 450 K, respectively,[14] but at those temperatures, the H4 and H5 peaks are still present in significant concentration.

IV. DISCUSSION

The results presented here clearly demonstrate the advantages gained from the improved emitter structure of the p/n InP solar cells in configuration C, fabricated by ERI. Because no suitable passivation scheme has yet been developed for InP, a thicker emitter generally results in an increased dark current contribution from the emitter and, hence, a reduced V_{oc}. This is evident in the fact that the configurations A and C cells, with emitters that were only half as thick as the configuration B cells, displayed higher V_{oc} values. The configuration C cells displayed the highest V_{oc} values as a result of the $p+/p$ step-graded structure that minimized the Zn interstitial defect density while maintaining a low bulk resistivity in the emitter.[4] The largest improvement is seen in the carrier collection efficiency apparent in the QE and I_{sc} data. The configuration C cells display excellent photoresponse across the full wavelength range. This is especially true for the shorter wavelength light that is absorbed in the emitter where the electric field established by the step grade and the reduced Zn interstitial defect density result in significantly enhanced performance.

The radiation data presented here show that the p/n InP solar cells with improved as-grown performance also display good radiation resistance. The rate of degradation P_{max} under irradiation was found to be similar to that of a radiation hard n/p InP cell. Moreover, the P_{max} degradation rates of the three different p/n cell configurations were essentially equal, independent of the preirradiation performance. Thus, the improved performance of the configuration C cells is expected to be maintained in a space radiation environment. It should be noted that throughout the analysis, data measured after irradiation by protons of different energies have been successfully correlated in terms of Dd. Thus, the conclusions drawn here can be considered general in nature and are expected to accurately describe the cell response to irradiation by protons of any energy or by a spectrum of proton energies as encountered in the space radiation environment.

For Dd levels below about 2×10^{12} MeV/g, the primary radiation-induced degradation mechanism in the p/n InP cells is a decrease in the diffusion length. The base diffusion length values determined from the QE data from cells in configurations B and C are similar, so the base diffusion length damage coefficient determined from these data is expected to be generally applicable. The excellent emitter response of the configuration C cells allowed for an analysis of the emitter diffusion length as well.

At higher irradiation levels, additional damage mechanisms were seen to emerge, as more solar cell degradation was observed than could be accounted for by diffusion length degradation alone. Modeling of the EBIC data suggests a reduction in the base majority carrier concentration and mobility with a subsequent increase in resistivity (Figs. 11 and 12). These effects are typically interpreted as carrier removal, caused by radiation-induced defect levels acting as compensation centers, depleting and eventually type converting the base as has been shown explicitly for *p*-type InP[9] and *p*-type Si.[15] However, the present $C-V$ data (Fig. 13) showed a decreased slope of the $1/C^2$ vs V curve, suggesting an *increase* in carrier concentration. The EBIC sample of Fig. 11 experienced a much heavier irradiation than the $C-V$ sample, leaving the possibility of a carrier removal mechanism emerging with increased defect concentration. However, Weinberg *et al.*[16] and Sibille[17] have observed similar increases in capacitance in similar samples after irradiation up to a Dd levels as high as 2.3×10^{12} MeV/g, which they interpreted as an increase in the base majority charge carrier density.

In the model proposed by Sibille, the primary radiation-induced defect level, corresponding to the DLTS peak here labeled EB, is produced by a defect complex consisting of a positively charged, radiation-induced phosphorous vacancy (V_p^+) and an ionized Zn shallow acceptor (Zn_{In}^-). The shallow acceptor ions are present in the *n*-type base due to diffusion from the emitter. Sibille argues that when the defect

complex forms, the shallow acceptor level is pushed so deep into the forbidden gap that it re-emits trapped electrons within milliseconds at room temperature, thus appearing to act as a deep donor and increasing the majority charge carrier concentration. However, this does not explain the increase in resistivity that Weinberg *et al.* observed concurrently with the capacitance increase, and it is not consistent with the EBIC results presented here.[16]

To better understand these effects, it is noted that the junction capacitance is a measure of the space charge density created by the fixed, ionized dopant atoms, not the free charge carrier density itself. Therefore, it may be more appropriate to attribute the observed radiation-induced increase in capacitance to the relative increase in space charge density due to the neutralization of the Zn_{In}^{-} ions that occurs when the defect complex forms. The rapid electron emission from the defect level ensures the electrical neutrality of the defect. In this interpretation, the capacitance would increase without an actual increase in the majority charge carrier concentration. The mechanism for electron removal from the *n*-type material required to explain the increased resistivity observed in Ref. 16 and the present EBIC data would come from the isolated, radiation-induced V_p^+ defect acting as a deep electron trap (i.e., a compensation center). This defect is expected to be electrically neutral after electron capture, so it would not be expected to affect the junction capacitance. Also, it would not be statistically favorable for a large concentration of the isolated defect to exist until the concentration of Zn_{In}^{-} atoms had been exhausted, i.e., until after heavy irradiation. At such point, the defect concentration would be large enough to expect degradation of the mobility due to scattering. Thus, an increase in resistivity and decrease in mobility would be observed without a change in capacitance, in agreement with the measured results.

V. CONCLUSIONS

A detailed study of the radiation response of high efficiency p/n InP solar cells has been presented. The degradation of the cell PV response due to irradiation by protons of different energies has been correlated in terms of displacement damage dose, and a characteristic proton curve has been determined. The p/n cells were shown to display excellent radiation hardness. The radiation-induced defect spectra have been characterized. Diffusion length degradation in the base and emitter primarily controlled the cell radiation response at lower Dd levels, and damage coefficients have been determined.

At higher Dd levels, radiation-induced increase in resistivity and decrease in mobility was observed along with a small increase in junction capacitance. By extending the model of Sibille,[17] a self-consistent model for these effects has been presented in which the primary radiation-induced phosphorous vacancy defect neutralizes ionized Zn atoms in the base region thereby increasing the space charge density. Once the Zn concentration in the base region has been exhausted, the primary radiation-induced defect remains isolated, acting as an electron trap that is electrically neutral when full of electrons thereby reducing the carrier concentration without altering the junction capacitance.

ACKNOWLEDGMENTS

The Office of Naval Research supported this work at NRL. The Comisión Interministerial de Ciencia y Tecnología (CICYT) under MAT94-0823-CO3-02 and the Junta de Andalucía through TEP-0120 supported this work in Spain.

[1] M. Yamaguchi and K. Ando, J. Appl. Phys. **63**, 5555 (1988).
[2] R. J. Walters, S. R. Messenger, H. L. Cotal, G. P. Summers, and E. A. Burke, Solid-State Electron. **39**, 797 (1996).
[3] R. J. Walters, S. R. Messenger, H. L. Cotal, M. A. Xapsos, S. J. Wojtczuk, H. B. Serreze, and G. P. Summers, J. Appl. Phys. **82**, 2164 (1997).
[4] R. W. Hoffman, Jr., N. S. Fatemi, P. P. Jenkins, V. G. Weizer, M. A. Stan, S. A. Ringel, D. A. Scheiman, D. M. Wilt, D. J. Brinker, R. J. Walters, and S. R. Messenger, Proc. IEEE 26th Photovoltaic Specialist Conference, Anaheim, CA, 30 Sept.–3 Oct. 1997, p. 815.
[5] M. J. Romero, Ph.D. thesis, University of Cadiz, 1999.
[6] G. P. Summers, E. A. Burke, and M. A. Xapsos, Radiat. Meas. **24**, 1 (1995).
[7] H. Y. Tada, J. R. Carter, B. E. Anspaugh, and R. G. Downing, *The Solar Cell Radiation Handbook* (JPL Publication, Pasadena, CA, 1982).
[8] C. J. Keavney, R. J. Walters, and P. J. Drevinsky, J. Appl. Phys. **73**, 60 (1993).
[9] S. R. Messenger, E. M. Jackson, E. A. Burke, R. J. Walters, M. A. Xapsos, and G. P. Summers, J. Appl. Phys. **86**, 1230 (1999).
[10] H. J. Hovel, *Semiconductors and Semimetals, Solar Cells*, edited by R. K. Willardson and A. C. Beer (Academic, New York, 1975), pp. 15–20.
[11] S. M. Sze, *Physics of Semiconductor Devices* (Wiley, New York, 1981), pp. 79–80.
[12] R. J. Walters and G. P. Summers, J. Appl. Phys. **69**, 6488 (1991).
[13] R. J. Walters, S. R. Messenger, H. L. Cotal, and G. P. Summers, J. Appl. Phys. **80**, 4315 (1996).
[14] M. J. Panunto, Ph.D. thesis University of Maryland, 1996.
[15] S. J. Taylor, M. Yamaguchi, M. Yang, M. Imaizumi, S. Matsuda, O. Kawasaki, and T. Hisamatsu, Appl. Phys. Lett. **70**, 2165 (1997).
[16] I. Weinberg, G. C. Rybicki, C. Vargas-Aburto, R. K. Jain, and D. Scheiman, Proceedings of the 13th Space Photovoltaic Research and Technology Conference, 14–16 June 1994, NASA Lewis Research Center, Cleveland, OH, NASA Publication #3278.
[17] A. Sibille, Appl. Phys. Lett. **48**, 593 (1986).